INSTITUTE OF PHYSICS PUBLISHING JOURNAL OF PHYSICS B: ATOMIC, MOLECULAR AND OPTICAL PHYSICS

J. Phys. B: At. Mol. Opt. Phys. **38** (2005) 3251–3271 doi:10.1088/0953-4075/38/17/014

Bound-state corrections in laser-induced nonsequential double ionization

C Figueira de Morisson Faria[1,2] **and M Lewenstein**[1,3,4]

[1] Institut für theoretische Physik, Universität Hannover, Appelstr. 2, D-30167 Hannover, Germany
[2] School of Engineering and Mathematical Sciences, City University, Northampton Square, London EC1V OHB, UK
[3] ICFO, Institut de Ciències Fotòniques, Jordi Girona 29, E-08034 Barcelona, Spain

Received 13 June 2005
Published 31 August 2005
Online at stacks.iop.org/JPhysB/38/3251

Abstract

We perform a systematic analysis of how nonsequential double ionization in intense, linearly polarized laser fields is influenced by the initial states in which both electrons are bound and by the residual ionic potential. We assume that the second electron is released by electron-impact ionization of the first electron with its parent ion, using an S-matrix approach. We work within the strong-field approximation and compute differential electron-momentum distributions using saddle-point methods. Specifically, we consider electrons in 1s, 2p, 3p and localized states, which are released by either a contact- or a Coulomb-type interaction. We also perform an adequate treatment of the bound-state singularity which is present in this framework. We show that the momentum distributions are very sensitive with respect to spatially extended or localized wavefunctions, but are not considerably influenced by their shapes. Furthermore, the modifications performed in order to overcome the bound-state singularity do not significantly alter the momentum distributions, apart from a minor suppression in the region of small momenta. The only radical changes occur if one employs effective form factors, which take into account the presence of the residual ion upon rescattering. If the ionic potential is of contact type, it outweighs the spreading caused by a long-range electron–electron interaction or by spatially extended bound states. This leads to momentum distributions which exhibit a very good agreement with the existing experiments.

1. Introduction

Within the last few years, nonsequential double ionization (NSDI) in strong, linearly polarized laser fields has attracted a great deal of attention, both experimentally and theoretically [1].

[4] Also at Institució Catalana di Recerca i Estudis Avançats, Spain.

This interest has been triggered by the outcome of experiments in which the momentum component parallel to the laser-field polarization could be resolved, either for the doubly charged ion [2] or for both electrons [3]. Indeed, the observed features, namely two circular regions along the parallel momenta $p_{1\parallel} = p_{2\parallel}$ peaked at $p_{1\parallel} = p_{2\parallel} = \pm 2\sqrt{U_\mathrm{p}}$, with U_p the ponderomotive energy, are a clear fingerprint of electron–electron correlation and can be explained by a simple, three-step rescattering mechanism [4]. Thereby, an electron leaves an atom through tunnelling ionization (the 'first step'), propagates in the continuum, being accelerated by the field (the 'second step'), and recollides inelastically with its parent ion (the 'third step'). In this collision, it transfers part of its kinetic energy to a second electron, which is then released.

From the theoretical point of view, there exist models, both classical [5–7] and quantum mechanical [8–14], based on such a mechanism, which qualitatively reproduce the above-mentioned features. They leave, however, several open questions. A very intriguing fact is that, for instance, a very good agreement with the experiments is obtained if the interaction through which the first electron is dislodged is of contact type, and if no Coulomb repulsion is taken into account in the final electron states. This agreement worsens if this interaction is modelled in a more refined way, considering either a more realistic, Coulomb-type interaction or final-state electron–electron repulsion. Specifically, in recent publications, such effects have been investigated in detail using both an S-matrix computation and a classical ensemble model, and have been interpreted in terms of phase-space and dynamical effects [12, 13]. This analysis has been performed within the strong-field approximation (SFA) [15], which mainly consists in neglecting the atomic binding potential in the propagation of the electron in the continuum, the laser field when the electron is bound or at the rescattering, and the internal structure of the atom in question.

Within this framework, the NSDI transition amplitude is written as a five-dimensional integral, with a time-dependent action and comparatively slowly varying prefactors. Such an integral is then solved using saddle-point methods. Apart from being less demanding than evaluating such an integral numerically [8, 9] or solving the time-dependent Schrödinger equation [16], these methods provide a clear space–time picture of the physical process in question. In particular, the results are interpreted in terms of the so-called 'quantum orbits'. Such orbits can be related to the orbits of classical electrons and have been extensively used in the context of above-threshold ionization, high-order harmonic generation [17] and, more recently, nonsequential double ionization [11–14].

The fact that, in [12, 13], the crudest approximation yields the best agreement with the experiments, seems to indicate that the presence of the residual ion, which is not taken into account, screens both the long-range interaction which frees the second electron and the final-state repulsion. This suggests that the presence of the ionic binding potential in the physical steps describing nonsequential double ionization, i.e., tunnelling, propagation and electron-impact ionization, should somehow be incorporated. Indeed, in recent studies, it was found that Coulomb focusing considerably influences the NSDI yield [18].

Another possibility is related to how the initial states in which the electrons are bound affect the electron-momentum distributions. Indeed, the poor agreement between the computations with the Coulomb interaction and the experiments may be related to the fact that 1s states have been used in this case, instead of states with a different shape or spatial symmetry, such as, for instance, p states. Furthermore, it may as well be that an additional approximation performed in [12, 13] for the contact interaction, namely to assume that it takes place at the origin of the coordinate system, contributes to the good agreement between theory and experiments in this case. Physically, this means that the spatial extension of the wavefunction of the second electron is neglected. Such an approximation has not been performed in the computations for

the Coulomb interaction discussed in [12, 13] and, till date, there exist no systematic studies of its influence in the context of NSDI.

In this paper, we investigate such effects in the simplest possible ways. First, we assume that both electrons are initially in hydrogenic 2p and in 3p states, instead of s states, as previously done [11–14]. One should note that, in contrast to helium, for which s states are more appropriate, p states yield a more realistic description of the outer-shell electrons in neon and argon, respectively. Since the two latter species are used in most experiments, the choice of p states is justified. This is included in the transition amplitude as a form factor and does not modify the saddle-point equations. In both p- and s-state cases, we consider that the bound-state wavefunction of the second electron is either localized at the origin or extends over a finite spatial range, for the contact and Coulomb interactions. This provides information on how the initial state of the *second* electron influences electron-impact ionization, and hence the NSDI yield.

A further improvement consists in overcoming the bound-state singularity, which is present in the saddle-point framework, and which has not been addressed in [12, 13]. For this purpose, we use a slightly modified action, with respect to that considered in [12, 13], so that the tunnelling process and the propagation of both electrons in the continuum are altered. Such corrections depend on the initial wavefunction of the *first* electron. Hence, they shed some light on how this wavefunction affects the electron-momentum distributions. In particular, we investigate how such corrections influence several features in the momentum distributions, such as their shapes, the cutoff energies or the contributions from different types of orbits to the yield.

Finally, we employ a modified form factor for the first electron, upon return, which takes into account the ionic potential. This is a first step towards incorporating the residual ion in our formalism. As it will be discussed subsequently, this provides a strong hint that the ion is important, in order to achieve a good agreement between theory and experiment.

The manuscript is organized as follows. In section 2, we provide the necessary theoretical background for understanding the subsequent discussions. In sections 3–5, we present our results and, finally, in section 6 we state our conclusions.

2. Background

2.1. Transition amplitude

The transition amplitude of the laser-assisted inelastic rescattering process responsible for NSDI, in the strong-field approximation and in atomic units, is given by

$$M = -\int_{-\infty}^{\infty} \mathrm{d}t \int_{-\infty}^{t} \mathrm{d}t' \int \mathrm{d}^3k\, V_{\mathbf{p}_j,\mathbf{k}} V_{\mathbf{k},0} \exp[\mathrm{i}S(t,t',\mathbf{p}_j,\mathbf{k})], \tag{1}$$

with the action

$$S(t,t',\mathbf{p}_j,\mathbf{k}) = -\frac{1}{2}\sum_{j=1}^{2}\int_{t}^{\infty}[\mathbf{p}_j+\mathbf{A}(\tau)]^2\,\mathrm{d}\tau - \frac{1}{2}\int_{t'}^{t}[\mathbf{k}+\mathbf{A}(\tau)]^2\,\mathrm{d}\tau + |E_{01}|t' + |E_{02}|t. \tag{2}$$

Equation (1) describes the following physical process: at a time t', both electrons are bound ($|E_{01}|$ and $|E_{02}|$ denote the first and second ionization potentials, respectively). Then, the first electron leaves the atom by tunnelling ionization and propagates in the continuum from the time t' to the time t, only under the influence of the external laser field $\mathbf{E}(t) = -\mathrm{d}\mathbf{A}(t)/\mathrm{d}t$. At this latter time, it returns to its parent ion with intermediate momentum $\mathbf{k}$ and gives part of its kinetic energy to the second electron through the interaction V_{12}, so that it is able to

overcome the second ionization potential $|E_{02}|$. Finally, both electrons reach the detector with final momenta $\mathbf{p}_j$ $(j = 1, 2)$. All the influence of the binding potential V and of the electron–electron interaction V_{12} is included in the form factors

$$V_{\mathbf{p}_j,\mathbf{k}} = \langle \mathbf{p}_2 + \mathbf{A}(t), \mathbf{p}_1 + \mathbf{A}(t)|V_{12}\big|\mathbf{k} + \mathbf{A}(t), \psi_0^{(2)}\rangle \tag{3}$$

and

$$V_{\mathbf{k},0} = \langle \mathbf{k} + \mathbf{A}(t')|V\big|\psi_0^{(1)}\rangle, \tag{4}$$

which are explicitly given by

$$V_{\mathbf{k},0} = \frac{1}{(2\pi)^{3/2}} \int \mathrm{d}^3 r_1 \exp[\mathrm{i}(\mathbf{k} + \mathbf{A}(t')) \cdot \mathbf{r}_1] V(\mathbf{r}_1)\psi_0^{(1)}(\mathbf{r}_1) \tag{5}$$

and

$$V_{\mathbf{p}_j,\mathbf{k}} = \frac{1}{(2\pi)^{9/2}} \int\int \mathrm{d}^3 r_1\, \mathrm{d}^3 r_2 \exp[\mathrm{i}(\mathbf{p}_1 - \mathbf{k}) \cdot \mathbf{r}_1] \exp[\mathrm{i}(\mathbf{p}_2 + \mathbf{A}(t)) \cdot \mathbf{r}_2] V_{12}(\mathbf{r}_2, \mathbf{r}_1)\psi_0^{(2)}(\mathbf{r}_2), \tag{6}$$

respectively. The binding potential $V(\mathbf{r}_1)$ will be taken to be of Coulomb type and the interaction $V_{12}(\mathbf{r}_2, \mathbf{r}_1)$ through which the second electron is released will be chosen to be of contact or Coulomb type. The initial state $\psi_0^{(1)}(\mathbf{r}_1)$ of the first electron at the moment of its ionization will be taken as a hydrogenic s or p state, and the wavefunction $\psi_0^{(2)}(\mathbf{r}_2)$ of the second electron at the moment of its release is either chosen as a hydrogenic state or a Dirac delta state localized at $\mathbf{r}_2 = 0$. In equation (1), we neglect final-state electron–electron repulsion (for a discussion of this effect, see [8, 13]).

2.2. Saddle-point analysis

We solve equation (1) applying the steepest descent method, which is a very good approximation for low enough frequencies and high enough driving-field intensities. In this case, we must find $\mathbf{k}$, t' and t so that $S(t, t', \mathbf{p}_n, \mathbf{k})$ $(n = 1, 2)$ is stationary, i.e., its partial derivatives with respect to these parameters vanish. This yields

$$[\mathbf{k} + \mathbf{A}(t')]^2 = -2|E_{01}|, \tag{7}$$

$$\sum_{j=1}^{2} [\mathbf{p}_j + \mathbf{A}(t)]^2 = [\mathbf{k} + \mathbf{A}(t)]^2 - 2|E_{02}|, \tag{8}$$

$$\int_{t'}^{t} \mathrm{d}\tau [\mathbf{k} + \mathbf{A}(\tau)] = 0. \tag{9}$$

Equation (7) gives the energy conservation during tunnelling ionization and, for a non-vanishing ionization potential, has no real solution. Consequently, t, t' and $\mathbf{k}$ are complex quantities. In the limit $|E_{01}| \to 0$, equation (7) describes a classical electron leaving the origin of the coordinate system with vanishing drift velocity. Equation (8) expresses energy conservation at t, in an inelastic rescattering process in which the first electron gives part of its kinetic energy to the second electron, so that it can overcome the second ionization potential and reach the continuum. Finally, equation (9) yields the intermediate electron momentum constrained by the condition that the first electron returns to the site of its release.

The saddles determined by equations (7)–(9) always occur in pairs that nearly coalesce at the boundaries of the energy region for which electron-impact ionization is allowed to

occur, within a classical framework. Such a boundary causes the yield to decay exponentially, leading to sharp cutoffs in the momentum distributions.

If written in terms of the momentum components parallel and perpendicular to the laser-field polarization, equation (8) reads

$$\sum_{j=1}^{2}[p_{j||}+A(t)]^2=[\mathbf{k}+\mathbf{A}(t)]^2-2|E_{02}|-\sum_{j=1}^{2}\mathbf{p}_{j\perp}^2 \tag{10}$$

and describes a hypersphere in the six-dimensional $(p_{j\parallel}, \mathbf{p}_{j\perp})$ space. This hypersphere delimits a region in momentum space for which electron-impact ionization is 'classically allowed', i.e., exhibits a classical counterpart. For constant transverse momenta, equation (10) corresponds to a circle in the $(p_{1||}, p_{2||})$ plane centred at $-A(t)$ and whose radius is given by the difference between the kinetic energy $E_{\mathrm{kin}}(t)=1/2[\mathbf{k}+\mathbf{A}(t)]^2$ of the first electron upon return and the effective ionization potential $|\tilde{E}_{02}|=|E_{02}|+\sum_{j=1}^{2}\mathbf{p}_{j\perp}^2/2$. Clearly, this radius is most extensive if the final transverse momenta $\mathbf{p}_{j\perp}$) $(j=1,2)$ are vanishing, such as in the examples provided in section 4.

In order to compute the transition probabilities, we employ a specific uniform saddle-point approximation, whose only applicability requirement is that the saddles occur in pairs [19, 21]. Unless stated otherwise (e.g., in section 4), we reduce the problem to two dimensions, using equation (9) and the fact that the action (2) is quadratic in $\mathbf{k}$. Details about this method, in the context of NSDI, are given in [11–14] (for above-threshold ionization and high-order harmonic generation, cf [19] and [20], respectively).

The momentum distributions of electrons for various types of interaction V_{12} read

$$M=\int \mathrm{d}^2 p_{1\perp}\int \mathrm{d}^2 p_{2\perp}|M_{\mathrm{L}}+M_{\mathrm{R}}|^2, \tag{11}$$

where the transverse momenta have been integrated over, and M_{L} and M_{R} give the left and right peaks in the momentum distributions, respectively, computed using the uniform approximation. We consider a monochromatic, linearly polarized field, so that the vector potential reads

$$\mathbf{A}(t)=-A_0\cos(\omega t)\mathbf{e}_x. \tag{12}$$

In this case, $M_{\mathrm{R}}=M(t,t',p)$ and $M_{\mathrm{L}}=M(t-T/2,t'-T/2,p)$, where $T=2\pi/\omega$ denotes a period of the driving field. We use the symmetry property $|M(t,t',p)|=|M(t-T/2,t'-T/2,-p)|$ to compute the left peak. One should note that, for other types of driving fields, such as few-cycle pulses, this condition does not hold and each peak must be computed independently [7, 14].

3. Initial p states

Within the formalism discussed in the previous section, the first and second electrons, so far, have been assumed to be initially in 1s or zero-range-potential bound states, whose energies $|E_{01}|$ and $|E_{02}|$ are taken to be the first and second atomic ionization potentials, respectively. In most experiments, however, species such as neon and argon are used, for which the outer-shell electrons are in 2p and 3p states, respectively. For this reason, such states should provide a more realistic modelling of laser-induced nonsequential double ionization. For symmetry reasons, only the states with magnetic quantum number $m=0$ will contribute to the yield.

In this case, the bound-state wavefunctions of both electrons will be given by

$$\psi_{210}^{(j)}(r_j)=C_{210}r_j\exp[-\alpha_j r_j]\cos\theta \tag{13}$$

and

$$\psi_{310}^{(j)}(r_j) = C_{310} r_j (1 - \alpha_j r_j/2) \exp[-\alpha_j r_j] \cos\theta, \tag{14}$$

respectively, where $\alpha_j = \sqrt{2|E_{0j}|}$ $(j = 1, 2)$ and C_{n10} (where n is the principal quantum number) denote normalization constants. For comparison, we will also consider hydrogenic 1s wavefunctions, which read

$$\psi_{100}{}^{(j)}(r_j) = C_{100} \exp[-\alpha_j r_j]. \tag{15}$$

In equations (13)–(15), the binding energies of the first and second electrons were chosen as the first and second ionization potentials, respectively.

The form factors $V_{\mathbf{p}_j,\mathbf{k}}$, for 2p and 3p initial states, read

$$V_{\mathbf{p}_j,\mathbf{k}}^{(2p)} \sim \eta(\mathbf{p}_1, \mathbf{k}) \frac{\tilde{p}}{[2|E_{02}| + \tilde{\mathbf{p}}^2]^3} + (\mathbf{p}_1 \leftrightarrow \mathbf{p}_2) \tag{16}$$

and

$$V_{\mathbf{p}_j,\mathbf{k}}^{(3p)} \sim \eta(\mathbf{p}_1, \mathbf{k}) \frac{\tilde{p}(\tilde{\mathbf{p}}^2 - 2|E_{02}|)}{[2|E_{02}| + \tilde{\mathbf{p}}^2]^4} + (\mathbf{p}_1 \leftrightarrow \mathbf{p}_2), \tag{17}$$

respectively, with $\tilde{\mathbf{p}} = \mathbf{p}_1 + \mathbf{p}_2 - \mathbf{k} + \mathbf{A}(t)$. Thereby, $(\mathbf{p}_1 \leftrightarrow \mathbf{p}_2)$ means that the momenta of both particles are interchanged, and $\eta(\mathbf{p}_j, \mathbf{k})$ $(j = 1, 2)$ is a function which depends on the interaction in question. The corresponding form factor obtained for an initial state (15) is given by

$$V_{\mathbf{p}_j,\mathbf{k}}^{(1s)} \sim \eta(\mathbf{p}_1, \mathbf{k}) \frac{1}{[2|E_{02}| + \tilde{\mathbf{p}}^2]^2} + (\mathbf{p}_1 \leftrightarrow \mathbf{p}_2). \tag{18}$$

3.1. Contact-type interaction

As a first step, we will assume that the second electron is released by a contact-type interaction

$$V_{12} \sim \delta(\mathbf{r}_1 - \mathbf{r}_2). \tag{19}$$

In this case, in equations (16)–(18), $\eta(\mathbf{p}_j, \mathbf{k})$ is a constant. The differential electron-momentum distributions computed with such form factors are depicted in figures 1(a)–(c), as contour plots in the $(p_{1||}, p_{2||})$ plane. In such computations, only the pair of orbits for which the electron excursion times $\tau = t - t'$ in the continuum are shortest have been employed. As an overall feature, the distributions are peaked near $p_{1||} = p_{2||} = \pm\sqrt{U_p}$ and spread in the direction perpendicular to the diagonal $p_{1||} = p_{2||}$.

An inspection of the form factors (16)–(18), for constant $\eta(\mathbf{p}_j, \mathbf{k})$, explains this behaviour. Indeed, such form factors are large if their denominator is small. Since $|E_{02}|$ is constant, this condition implies that $\tilde{\mathbf{p}} = \mathbf{p}_1 + \mathbf{p}_2 - \mathbf{k} + \mathbf{A}(t)$ is small. To first approximation, since the first electron returns at times t close to the minimum of the electric field, one may assume that the vector potential at this time and the intermediate electron momentum are approximately constant. Furthermore, in the model, the field is approximated by a monochromatic wave and $\mathbf{k}$ is given by equation (9). Hence, a rough estimate of these quantities at the return times yields $A(t) \simeq 2\sqrt{U_p}$ and $k \simeq 0$, respectively. Thus, $\tilde{\mathbf{p}}$ will be small mainly if $\mathbf{p}_1 = -\mathbf{p}_2$, so that contributions along the anti-diagonal $p_{1||} = -p_{2||}$ will be enhanced.

Such contributions get more localized near the maxima for highly excited initial states due to the increase in the exponent of the denominator. A direct look at the above-stated form factors confirms this interpretation, yielding maxima along the anti-diagonal and near $\pm\sqrt{U_p}$.

Interestingly, the distributions obtained for the contact interaction are quite different from the circular distributions peaked around $p_{1||} = p_{2||} = \pm 2\sqrt{U_p}$ observed experimentally.

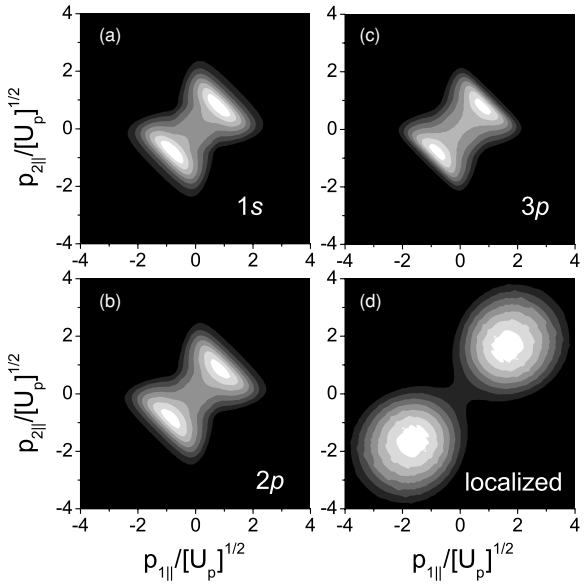

Figure 1. Electron-momentum distributions computed using a contact-type interaction, as functions of the electron-momentum components parallel to the laser-field polarization. The external field was taken to be monochromatic, with frequency $\omega = 0.057$ au and intensity $I = 8 \times 10^{14}$ W cm^{-2} ($U_p = 1.75$ au). In panels (a), (b) and (c), both electrons are initially bound in 1s, 2p and 3p states (equations (15), (13) and (14)), respectively, whereas in part (d) the first electron is initially in a 1s state and the wavefunction of the second electron is localized at $r_2 = 0$. In all situations (even for the 3p-state case), the atomic species was taken to be neon ($|E_{01}| = 0.79$ au and $|E_{02}| = 1.51$ au), in order to facilitate a clear assessment of the effects caused by the different initial states. The transverse momenta have been integrated over.

Indeed, in order to obtain such distributions, it is necessary to assume that the initial wavefunction of the second electron is localized at $r_2 = 0$. This is formally equivalent to taking

$$V_{12}(\mathbf{r}_1 - \mathbf{r}_2)\psi_0^{(2)}(\mathbf{r}_2) \sim \delta(\mathbf{r}_1 - \mathbf{r}_2)\delta(\mathbf{r}_2). \tag{20}$$

Equation (20) yields a constant form factor $V_{\mathbf{p}_j,\mathbf{k}}$. In figure 1(d), we present the distributions computed using equation (20), which exhibit a very good agreement with the experiments. This means that, in reality, the effective wavefunction of the second electron is very localized, most probably due to refocusing [18] or screening effects [22].

3.2. Coulomb-type interaction

We will now consider that the second electron is released by a Coulomb-type interaction, given by

$$V_{12} = 1/|\mathbf{r}_1 - \mathbf{r}_2|. \tag{21}$$

In this case, in the form factors (16)–(18), η is given by

$$\eta(\mathbf{p}_j, \mathbf{k}) = \frac{1}{[\mathbf{p}_j - \mathbf{k}]^2} \qquad (j = 1, 2), \tag{22}$$

respectively. This causes the prefactors to be large when $\mathbf{p}_j - \mathbf{k}$ ($j = 1, 2$) is small, in addition to the case for which $\tilde{\mathbf{p}} \ll 1$. The influence of such form factors on the electron-momentum distributions is shown in figure 2. Apart from the broadening along $p_{1||} = -p_{2||}$

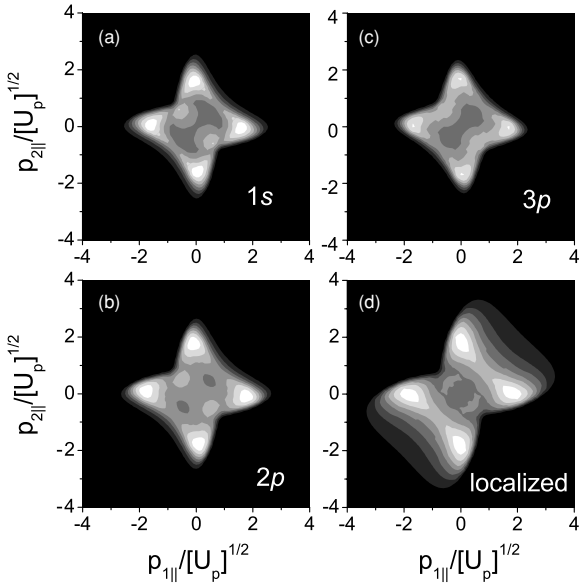

Figure 2. Electron-momentum distributions computed using a Coulomb-type interaction, as functions of the electron-momentum components parallel to the laser-field polarization. The field and atomic parameters are the same as in figure 1. In panels (a), (b) and (c), both electrons are taken to be initially in 1s, 2p and 3p states, respectively, whereas in panel (d) the first electron is in a 1s state, while the spatial extension of the bound-state wavefunction has been neglected. The transverse momenta have been integrated over.

caused by the spatial extent of the bound-state wavefunctions (cf section 3.1), the distributions exhibit maxima near the axis $p_{1||} = 0$ or $p_{2||} = 0$. Such maxima are due to the factor (22) in equations (16)–(18), characteristic of the Coulomb-type interaction, which is large for $\mathbf{p}_j \simeq \mathbf{k}$. Since, to first approximation, contributions from regions of small k dominate the yield, one expects maxima in momentum regions where either $\mathbf{p}_1$ or $\mathbf{p}_2$ are small.

Furthermore, as compared to the yields obtained using a Coulomb-type interaction and 1s states, there exists a small additional broadening in the distributions, with respect to the diagonal $p_{1||} = p_{2||}$, as well as an increase in the contributions from regions where such momenta are small. Such effects get more pronounced as the principal quantum number increases, as shown in figures 2(b) and (c).

However, such modifications do not alter the distributions in a significant way. More extreme changes occur, for instance, if a contact-type interaction, i.e., $\eta(\mathbf{p}_j, \mathbf{k}) =$ constant in equation (19), is taken into account. Still, less localized bound states for both electrons will cause a broadening in the momentum distributions. If the second-electron wavefunction is localized at the origin, the form factor (18) reduces to

$$V_{\mathbf{p}_j,\mathbf{k}} \sim \frac{1}{[\mathbf{p}_1 - \mathbf{k}]^2} + (\mathbf{p}_1 \leftrightarrow \mathbf{p}_2). \tag{23}$$

The distributions for the latter form factor are displayed in figure 2(d). In the figure, one observes a considerable reduction of the broadening along the anti-diagonal $p_{1||} = -p_{2||}$. However, the distributions still exhibit the two sets of maxima near the axis $p_{1||} = 0$ or $p_{2||} = 0$. This is expected, since such maxima are a fingerprint of the Coulomb interaction.

The results in this section show that the shapes of the momentum distributions in NSDI are not only influenced by the type of interaction by which the second electron is dislodged

but, additionally, depend on the spatial extension of the wavefunction of the state where it is initially bound. In fact, radically different shapes are observed if this wavefunction is either taken to be localized at $\mathbf{r}_2 = 0$ or exponentially decaying. This is true both for a contact- and a Coulomb-type interaction (cf figures 1(d) and 2(d)).

On the other hand, if different initial states are taken, for the same type of interaction, there are no significant changes in the shapes of the distributions as long as such states extend over a finite spatial range. This is explicitly seen by comparing yields obtained using bound states with different principal quantum numbers. This is related to the fact that the wavefunctions (13)–(15) were chosen such that the bound-state energy always corresponds to the second ionization potential. Hence, even if their shape changes, the spatial extension of such wavefunctions is roughly the same.

It is still, however, quite puzzling that the best agreement with the experimental findings occurs for the crudest approximations, both for the interaction and the initial bound-state wavefunction, i.e., for a contact-type interaction and a wavefunction localized at $\mathbf{r}_2 = 0$. Indeed, taking either a more realistic type of electron–electron interaction, spatially extended bound states, or, still, bound states which are, in principle, a more refined description of the outer-shell electrons, only worsens the agreement between experiment and theory.

If the main physical mechanism of NSDI is electron-impact ionization, there exist two main possibilities for explaining this discrepancy. Either the second electron is bound in a highly localized state and both electrons collide through an effective short-range interaction, as the present results suggest, or the tunnelling ionization, as well as the electron propagation in the continuum, must be improved. The first issue may be addressed by including the influence of the residual ion in the process, whereas the second issue may be dealt with in several ways. For instance, in the subsequent section, we will consider corrections of a more fundamental nature, which alter the semi-classical action and thus the orbits of the electrons.

4. Treatment of the bound-state singularity

Up to the present section, we have implicitly assumed that the form factors $V_{\mathbf{p}_j,\mathbf{k}}$ and $V_{\mathbf{k},0}$ are free of singularities and slowly varying in comparison to the time-dependent action. However, this is not always true. Indeed, in the saddle-point framework, the form factor $V_{\mathbf{k},0}$ is singular if the electron is initially in a state described by an exponentially decaying wavefunction, such as equations (13)–(15). More specifically, in this case,

$$V_{\mathbf{k},0} \propto \frac{f(k + A(t'))}{([\mathbf{k} + \mathbf{A}(t')]^2 + 2|E_{01}|)^n}, \tag{24}$$

where n is an integer number. In this case, according to equation (7), the denominator vanishes. Due to this singularity, this form factor does not vary slowly with respect to the semi-classical action (2) and thus must be incorporated in the exponent. Therefore, we take the modified action

$$\tilde{S}(t, t', \mathbf{p}_j, \mathbf{k}) = S(t, t', \mathbf{p}_j, \mathbf{k}) - \mathrm{i} \ln[V_{\mathbf{k},0}] \tag{25}$$

in the transition amplitude (1). This causes a change in the first and third saddle-point equations, which will depend on the initial bound state in question. In particular, we will consider that the first electron is initially in the hydrogenic states 1s, 2p and 3p. This is a legitimate assumption, since the binding potential of a neutral atom, from which the first electron tunnels out, is of long-range type. For the states 1s, 2p and 3p, $V_{\mathbf{k},0}$ reads

$$V_{\mathbf{k},0}^{(1s)} = \frac{\sqrt{2}}{\pi} \frac{(2|E_{01}|)^{5/2}}{\mathbf{v}^2 + 2|E_{01}|}, \tag{26}$$

$$V_{\mathbf{k},0}^{(2p)} = \frac{2\sqrt{2}\mathrm{i}}{\pi}\frac{(\sqrt{2|E_{01}|})^{5/2}v}{(\mathbf{v}^2+2|E_{01}|)^2} \tag{27}$$

and

$$V_{\mathbf{k},0}^{(3p)} = \frac{8\mathrm{i}(\sqrt{2|E_{01}|})^{5/2}v(\mathbf{v}^2-2|E_{01}|)}{\sqrt{3}\pi(\mathbf{v}^2+2|E_{01}|)^3}, \tag{28}$$

respectively, where $\mathbf{v} = [\mathbf{k} + \mathbf{A}(t')]$ denotes the initial electron drift velocity. The explicit expressions for the saddle-point equations then become

$$[\mathbf{k} + \mathbf{A}(t')]^2 = -2|E_{01}| + \boldsymbol{\zeta}(k, t') \cdot \mathbf{E}(t') \tag{29}$$

and

$$\int_{t'}^{t} \mathrm{d}\tau [\mathbf{k} + \mathbf{A}(\tau)] + \boldsymbol{\zeta}(k, t') = 0, \tag{30}$$

respectively, where $\boldsymbol{\zeta}(k, t') = -\mathrm{i}\partial_{\mathbf{k}} \ln[V_{\mathbf{k},0}]$ is a correction which depends on the initial bound state. Thus, there is an effective shift in the ionization potential at the tunnelling times and a modification in the return condition. Consequently, the orbits change. Apart from that, from the technical point of view, the transition amplitude is no longer reducible to a two-dimensional integral, so that the problem is far more cumbersome.

The modifications in the equation describing tunnelling ionization allow the existence of solutions for which $\mathrm{Re}[v] \neq 0$. This did not occur in equation (7), for which this quantity was purely imaginary and, physically, means that there are in principle changes, maybe even enhancements, in the probability that the first electron tunnels out at t'.

Furthermore, equation (30), if written in terms of the components of the intermediate momentum $\mathbf{k}$ parallel and perpendicular to the laser-field polarization, has, apart from the trivial solution $\mathbf{k}_\perp = 0$, additional solutions for which $\mathbf{k}_\perp \neq 0$. Thus, in principle, the first electron may have, during the tunnel ionization and upon return, a non-vanishing drift-velocity component transverse to the laser-field polarization. We regard this possibility, however, as non-physical, and therefore will mainly concentrate on the case of vanishing $\mathbf{k}_\perp$. Despite of that, the results obtained for non-vanishing $\mathbf{k}_\perp$ will be briefly discussed in section 4.2. For the return condition (8), this is not possible and $\mathbf{k}_\perp$ is always vanishing. In the following, we will investigate how the corrections in the action affect the momentum distributions.

4.1. Vanishing $\mathbf{k}_\perp$

In this section, we will consider that the first electron has vanishing intermediate-momentum components $\mathbf{k}_\perp$. Physically, this means that the dynamics of NSDI is mainly taking place along the laser-field polarization, which is the intuitively expected situation. In figure 3, we present the electron-momentum distributions computed employing the modified saddle-point equations and the action (25), for the same initial states and types as in figure 1 and a contact-type interaction. In general, the distributions in figure 3 are very similar to the former ones, with, however, a suppression in the region of small parallel momenta. This is true even if different corrections are taken into account, as it is the case if the first electron is initially in 1s, 2p and 3p states (figures 3(a), (b) and (c), respectively). In the specific case of a localized bound-state wavefunction for the second electron, there is also a minor displacement of the maxima towards smaller parallel momenta (cf figure 3(d)).

The suppression persists if the second electron is released by a Coulomb-type interaction, as shown in figure 4. Specifically for this interaction, the corrections lead to a suppression of the secondary maxima in the small-momentum region, which were present in figure 2.

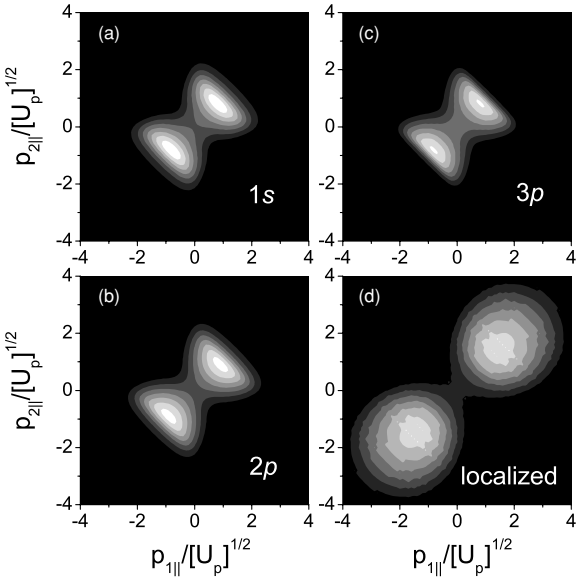

Figure 3. Electron-momentum distributions computed with using contact-type interaction, as functions of the electron-momentum components parallel to the laser-field polarization, for the same field and atomic parameters as in the previous figures. We introduce corrections to the bound-state singularity by employing the modified action (25) and saddle-point equations, taking the solutions displayed in figures 6(a) and (c). In panels (a), (b) and (c), both electrons are taken to be initially in 1s, 2p and 3p states, respectively, whereas in panel (d) the first electron is initially in a 1s state, while the spatial extension of the bound-state wavefunction of the second electron has been neglected. The transverse momenta have been integrated over.

In the following, we will analyse these differences in terms of the so-called quantum orbits, obtained by solving the saddle-point equations. We will consider both the saddle-point equations in the presence and absence of corrections to the bound-state singularity, i.e., equations (29), (8) and (30), and (7)–(9), respectively. We restrict ourselves to vanishing final transverse momenta and longitudinal momentum components along the diagonal $p_{||} = p_{1||} = p_{2||}$. For this particular case, the energy region for which electron-impact ionization is classically allowed is most extensive.

In figure 5, we display the solutions of the saddle-point equations for the rescattering times t and the intermediate momentum $\mathbf{k}$. The upper and lower panels in the figure give the real and imaginary parts of such variables, respectively. The real parts of t and $\mathbf{k}$ correspond to the solutions of the equations of motion of a classical electron in an external laser field, and almost merge at two distinct parallel momenta. These momenta are related to the maximal and minimal energy for which the second electron is able to overcome $|E_{02}|$. Beyond such momenta, there are cutoffs in the distributions, and the yield decays exponentially. The imaginary parts of such variables are in a sense a measure of a particular physical process being classically allowed or forbidden. Indeed, the fact that |Im| and |Im[k]| are vanishingly small between the minimal and maximal allowed momenta are a consequence of both electron-impact ionization and the return condition being classically allowed in this region. As the boundaries of this region are reached, |Im| and |Im[k]| increase exponentially. Interestingly, both the real and imaginary parts of such variables, as well as the cutoff momenta, remain practically unaltered upon the changes introduced in this section. This is not obvious, since the bound-state corrections in question alter the return condition (cf equation (30)).

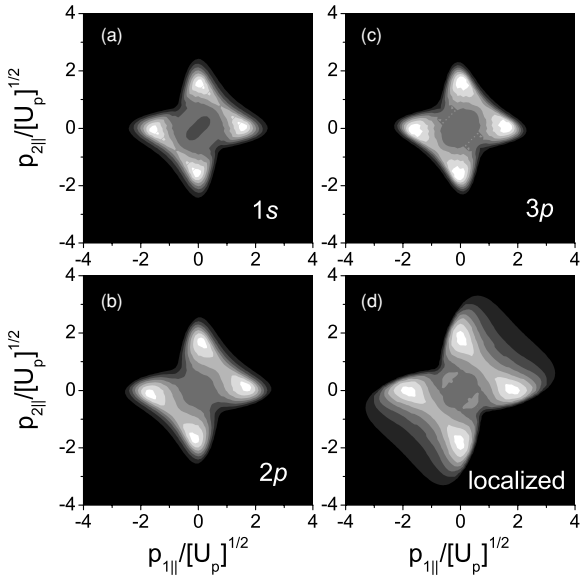

Figure 4. Electron-momentum distributions computed using the Coulomb-type interaction, as functions of the electron-momentum components parallel to the laser-field polarization, for the same field and atomic parameters as in the previous figures. We introduce corrections to the bound-state singularity by employing the modified action (25) and saddle-point equations, and the solutions in figures 6(a) and (c). In panels (a), (b) and (c), both electrons are taken to be initially in 1s, 2p and 3p states, respectively, whereas in panel (d) the first electron is initially in a 1s state, while the spatial extension of the bound-state wavefunction of the second electron has been neglected. The transverse momenta have been integrated over.

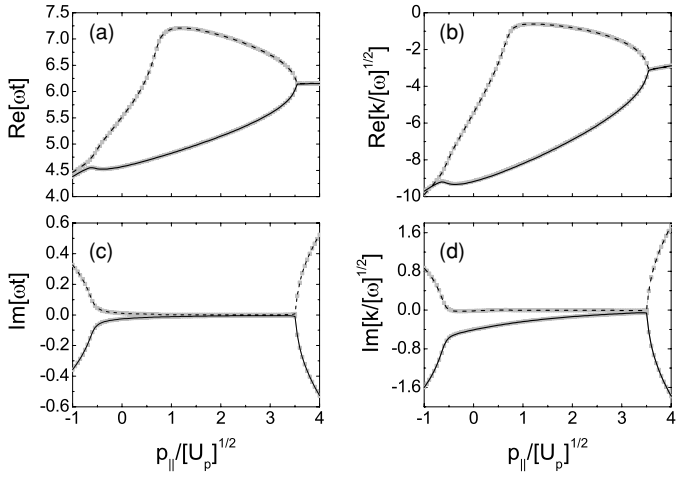

Figure 5. Rescattering times, together with the intermediate momentum $k_{||}$, as functions of the parallel momentum $p_{||}$ along the diagonal $p_{1||} = p_{2||}$. The final transverse momenta $\mathbf{p}_{j\perp}$ $(j = 1, 2)$ and the intermediate transverse momentum $\mathbf{k}_\perp$ are taken to be vanishing. The real and imaginary parts of such quantities are displayed in the upper (a)–(c) and lower (d)–(f) panels, respectively. The field and atomic parameters are the same as in the previous figures. The uncorrected variables are given by the thick light grey curves in the figure, while the variables with corrections corresponding to initial 1s, 2p and 3p states are given by the grey, dark grey and black curves, respectively. The longer and shorter orbits are indicated by dashed and solid lines, respectively.

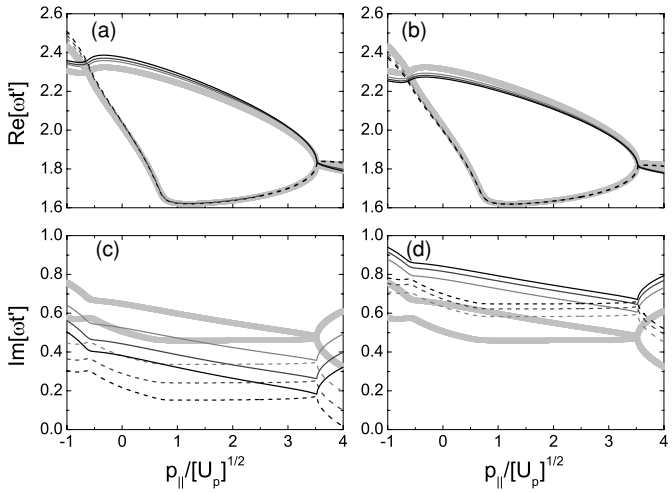

Figure 6. Tunnelling times as functions of the parallel momentum $p_{||}$ along the diagonal $p_{1||} = p_{2||}$. The final transverse momenta $\mathbf{p}_{j\perp}$ $(j = 1, 2)$ and the intermediate transverse momentum $\mathbf{k}_\perp$ are taken to be vanishing. The real and imaginary parts of such quantities are displayed in the upper (a and b) and lower (c and d) panels, and the same pairs of orbits are depicted in the left (a and c) and right (b and d) panels, respectively. The field and atomic parameters are the same as in the previous figures. The uncorrected variables are given by the thick light grey curves in the figure, while the variables with corrections corresponding to initial 1s, 2p and 3p states are given by the grey, dark grey and black curves, respectively. The longer and shorter orbits are indicated by dashed and solid lines, respectively.

There exist, however, modifications in the tunnelling times t', which are explicitly shown in figure 6. Specifically, the corrections in the tunnelling condition, which leads to equation (29), cause a splitting in the solutions of equation (7). This follows from the fact that small variations in the stationary-action trajectories contribute quadratically to $S(t, t', \mathbf{p}_j, \mathbf{k})$ and $V_{\mathbf{k},0}$, so that $\tilde{S}(t, t', \mathbf{p}_j, \mathbf{k})$ attains two stationary trajectories for each of the former ones. Strictly speaking, a similar splitting also occurs for $\mathbf{k}$ and t. In practice, however, the difference between the two different sets of solutions is vanishingly small and thus not noticeable in figure 5. The different sets of solutions are depicted in figures 6(a) and (c), and (b) and (d), respectively. The real parts Re$[t']$ exhibit only minor differences, which occur for the shorter orbits and small momenta and eventually disappear as the upper cutoff is approached. Depending on the type of correction, such times either distance themselves from, or become slightly closer to the peak-field times (figures 6(a) and (b), respectively). Thus, one could expect an enhancement in the contributions from the shorter orbits near the origin of the $(p_{1||}, p_{2||})$ plane, in the former case, and a suppression in the latter case. However, we have used the solutions in figures 6(b) and (d) for computing the contour plots in figures 3 and 4, and obtained a suppression in the yield. This is a clear indication that the changes in Im$[t']$ and in the time-dependent action play a more important role than those in Re$[t']$.

In figures 6(c) and (d), we present the imaginary parts of t', which clearly shift towards smaller and larger values, respectively, when the corrections $\varsigma(k, t')$ are taken into account. The higher the initial state lies, the larger such shifts are. Physically, there exists a correspondence between such imaginary parts and the probability that the first electron tunnels out and reaches the continuum. This means that, by using a slightly modified action in order to overcome the Coulomb singularity, one is changing the effective potential barrier at t' for the first electron. In general, such a barrier has a significant influence on the distributions. Indeed, recently,

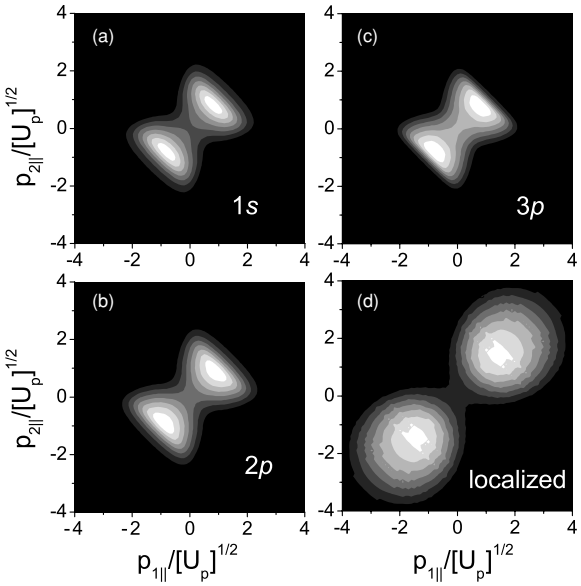

Figure 7. Electron-momentum distributions computed with the contact-type interaction, as functions of the electron-momentum components parallel to the laser-field polarization, for the same field and atomic parameters as in the previous figures. We introduce corrections to the bound-state singularity by employing the modified action (25) and saddle-point equations, taking the solutions in figures 6(b) and (d). In panels (a), (b) and (c), both electrons are taken to be initially in 1s, 2p and 3p states, respectively, whereas in panel (d) the first electron is in a 1s state, while spatial extension of the bound-state wavefunction of the second electron has been neglected. The transverse momenta have been integrated over.

we have shown, within the context of nonsequential double ionization with few-cycle laser pulses, that the importance of the contributions of a particular orbit or set of orbits to the yield is highly dependent on $|\mathrm{Im}[t']|$. The smaller this quantity is, the larger is the tunnelling probability for the first electron [14]. As a direct consequence, contributions from orbits with small $|\mathrm{Im}[t']|$, i.e., with a large tunnelling probability, dominate the yield. In the present case, however, since both orbits are being equally shifted, this should not influence the distributions qualitatively. One should note that, even in the momentum region for which electron-impact ionization is allowed, $|\mathrm{Im}[t']|$ is always non-vanishing. This is a direct consequence of the fact that tunnelling ionization is a classically forbidden process.

Subsequently, we compute the counterparts of figure 3 and 4 (figures 7 and 8) using the solutions displayed in figures 6(b) and (d). Also in this case, in general, there is a suppression in the yield in the region of small parallel momenta, with, however, a slightly different substructure in the Coulomb-interaction case.

4.2. Non-vanishing $\mathbf{k}_\perp$

The modifications introduced in the return condition for the first electron (equation (30)) allow the intermediate momentum $\mathbf{k}$ to have a non-vanishing component perpendicular to the laser-field polarization. This implies that the first electron, during tunnelling ionization and when it returns, is being deviated from its original direction. Although such an effect is unphysical, we will briefly discuss its consequences. For that purpose, we will consider the simplest corrections to the bound-state singularity discussed in this paper, namely those for 1s initial

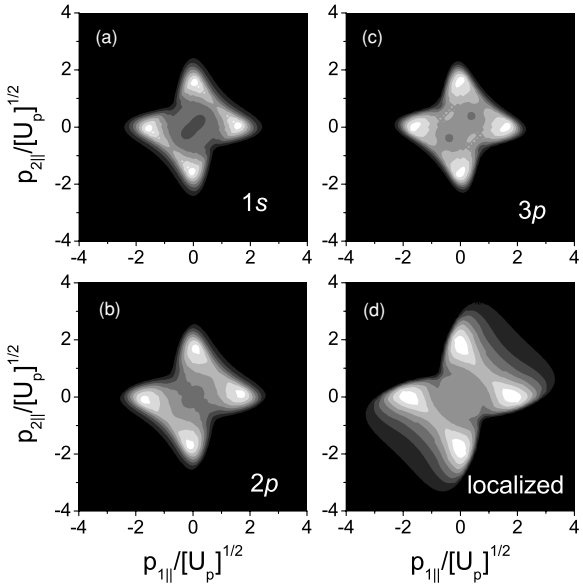

Figure 8. Electron-momentum distributions computed using the Coulomb-type interaction, as functions of the electron-momentum components parallel to the laser-field polarization, for same field and atomic parameters as in the previous figures. We introduce corrections to the bound-state singularity by employing the modified action (25) and saddle-point equations, and the solutions in figures 6(b) and (d). In panels (a), (b) and (c), both electrons are taken to be initially in 1s, 2p and 3p states, respectively, whereas in panel (d) the first electron is initially in a 1s state, while the spatial extension of the bound-state wavefunction of the second electron has been neglected. The transverse momenta have been integrated over.

states. If equation (30) is written in terms of the intermediate-momentum components $\mathbf{k}_\perp$ and $k_{||}$ perpendicular and parallel to the laser-field polarization, this equation reads

$$k_{||}(t-t') - \int_{t'}^{t} A(s)\,\mathrm{d}s + \frac{2\mathrm{i}[k_{||}+A(t')]}{[2|E_{01}|+\mathbf{k}_\perp^2+[k_{||}+A(t')]^2]} = 0 \tag{31}$$

and

$$\mathbf{k}_\perp^2\left(t-t'+\frac{2\mathrm{i}}{[2|E_{01}|+\mathbf{k}_\perp^2+[k_{||}+A(t')]^2]}\right) = 0, \tag{32}$$

respectively. Apart from the trivial solution $\mathbf{k}_\perp = 0$, condition (32) can be satisfied by non-vanishing values of this variable. One should note that, in the case without corrections, this does not hold and only the trivial solution exists.

Figure 9 depicts the tunnelling and rescattering times for this case, together with the perpendicular and parallel components of $\mathbf{k}$. The real parts of such variables correspond, as in the previous cases, to a longer and a shorter orbit. The momenta, however, for which such orbits nearly coalesce, are radically different from those in the previous cases discussed in this paper. This is due to the fact that a non-vanishing $\mathbf{k}_\perp$ also affects the rescattering condition (8), which now reads

$$\sum_{j=1}^{2}[p_{j||}+A(t)]^2 = [k_{||}+A(t)]^2+\mathbf{k}_\perp^2-2|E_{02}|-\sum_{j=1}^{2}\mathbf{p}_{j\perp}^2.$$

For constant final transverse momenta $\mathbf{p}_{j\perp}$ $(j=1,2)$, this equation describes a circle centred at $-A(t)$ whose radius has been altered in $\mathbf{k}_\perp^2$. Since, as shown in figures 9(a)–(d), this radius

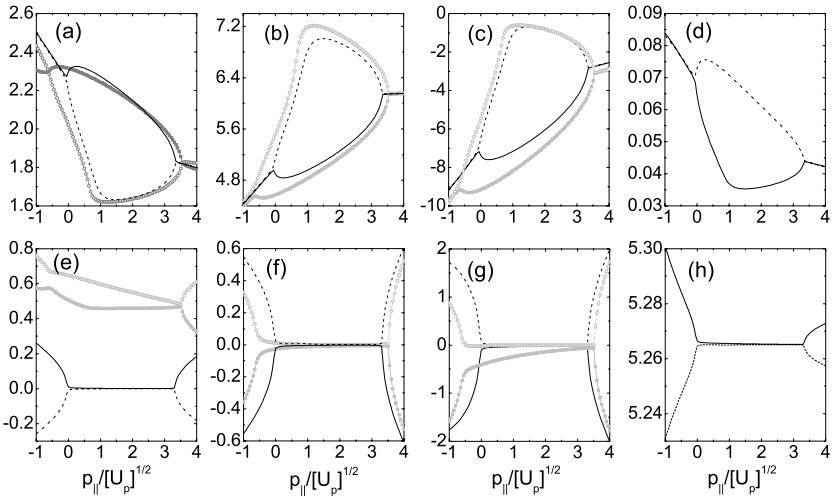

Figure 9. Tunnelling (a and e) and rescattering times (b and f), together with the parallel (c and g) and perpendicular components of the intermediate momentum **k** (d and h), as functions of the parallel momentum $p_{||}$ along the diagonal $p_{1||} = p_{2||}$. The final transverse momenta $\mathbf{p}_{j\perp}$ ($j = 1, 2$) are taken to be vanishing. The real and imaginary parts of such quantities are displayed in the upper (a)–(d) and lower (e)–(h) panels, respectively. The field and atomic parameters are the same as in the previous figures. The corrected and uncorrected yields are given by the black and grey curves in the figure, respectively. The tunnelling and rescattering times are multiplied by ω and the intermediate momenta divided by $\sqrt{\omega}$, respectively, so that a direct comparison with figures 5 and 6 can be performed.

decreased, $\mathbf{k}_\perp$ is expected to be almost purely imaginary. This is indeed the case, as can be seen comparing panels (d) and (h) in the figure. The imaginary parts of such variables also behave following the same pattern as previously, growing vary rapidly at the momenta for which the real parts approach each other, and remaining nearly constant in between. Interestingly, Im[t'] is vanishing in this region. This feature is in clear contradiction with the fact that tunnelling is a process which is always forbidden, and therefore requires a non-vanishing Im[t'] (cf figures 6(c) and (d)). For this reason, we will not use solutions with non-vanishing $\mathbf{k}_\perp$ for computing electron-momentum distributions.

5. Influence of the ion

In this section, we take a first step towards including the residual ion in our formalism. For that purpose, we consider an effective interaction $\widetilde{V} = V_{12} + V_{\rm ion}$ at the time the first electron returns, where $V_{\rm ion}$ is the ionic potential. Physically, this means that the first electron interacts not only with the electron it releases, but, additionally, with the residual ion. We take this potential to be of either Coulomb or contact type, and assume that only the two active electrons contribute to the ionic charge. Thus, explicitly, $V_{\rm ion}$ reads

$$V_{\rm ion}^{(\rm C)} = -2/|\mathbf{r}_1| \tag{33}$$

or

$$V_{\rm ion}^{(\delta)} \sim -2\delta(\mathbf{r}_1). \tag{34}$$

In this context, both the effective charge and a contact-type interaction are justified by the fact that the remaining electrons are screening the charge and the long-range tail of the binding potential.

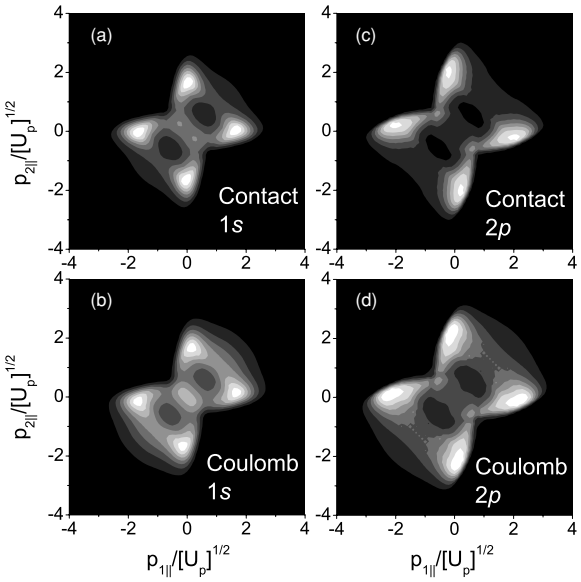

Figure 10. Electron-momentum distributions computed with the modified form factors (35) and (36), as functions of the electron-momentum components parallel to the laser-field polarization, for same field and atomic parameters as in the previous figures. We consider that the ionic potential is of Coulomb type (equation (33)), and use the saddle-point model without modifications (cf section 2). In the upper and lower panels, the electron–electron interaction V_{12} was assumed to be of contact and Coulomb types, respectively. In panels (a) and (b), both electrons are taken to be initially in 1s states, whereas in panels (c) and (d), they are initially in 2p states. The transverse momenta have been integrated over.

In equation (1), the form factors $V_{\mathbf{p_j},\mathbf{k}}$ are given by

$$\widetilde{V}^{(1s)}_{\mathbf{p}_j,\mathbf{k}} \sim V^{(1s)}_{\mathbf{p}_j,\mathbf{k}} - \frac{2\eta(\mathbf{p}_1,\mathbf{k})}{[2|E_{02}| + (\mathbf{p}_2 + \mathbf{A}(t))^2]^2} + (\mathbf{p}_1 \leftrightarrow \mathbf{p}_2), \tag{35}$$

$$\widetilde{V}^{(2p)}_{\mathbf{p}_j,\mathbf{k}} \sim V^{(2p)}_{\mathbf{p}_j,\mathbf{k}} - \frac{2\eta(\mathbf{p}_1,\mathbf{k})\sqrt{(\mathbf{p}_2 + \mathbf{A}(t))^2}}{[2|E_{02}| + (\mathbf{p}_2 + \mathbf{A}(t))^2]^3} + (\mathbf{p}_1 \leftrightarrow \mathbf{p}_2), \tag{36}$$

for 1s and 2p states, respectively. The prefactor V_{12} is of contact or Coulomb type. Furthermore, for a Coulomb or contact ionic potential, η is either constant or given by equation (22), respectively. In order to simplify the computations, and since only minor differences have been observed in this case, we use the model in section 2, instead of the more rigorous approach of section 4 in the subsequent figures.

Figure 10 depicts how the ion affects the electron-momentum distributions, if its potential is assumed to be of Coulomb form (equation (33)). The upper and lower panels have been computed for V_{12} of contact and Coulomb types, respectively. In the figure, the distributions resemble those obtained for the Coulomb-type interaction, if the second state is in a localized state (figures 2(d), 4(d) and 8(d)). This holds both for 1s and 2p initial electron states. An inspection of equations (35) and (36) explains this shape. Indeed, in both equations, the functional form of $\eta(\mathbf{p}_j, \mathbf{k})$, which is characteristic of long-range interactions, favours unequal momenta, leading to patterns similar to those observed in figures 2, 4 and 8. Furthermore, in the second terms in $\widetilde{V}_{\mathbf{p}_j,\mathbf{k}}$, the denominators are small if $\mathbf{p}_j \simeq -\mathbf{A}(t)$. Thus, since $A(t) \sim 2\sqrt{U_\mathrm{p}}$, we expect the form factors (35) and (36) to be large near $p_{2||} = p_{1||} = \pm 2\sqrt{U_\mathrm{p}}$.

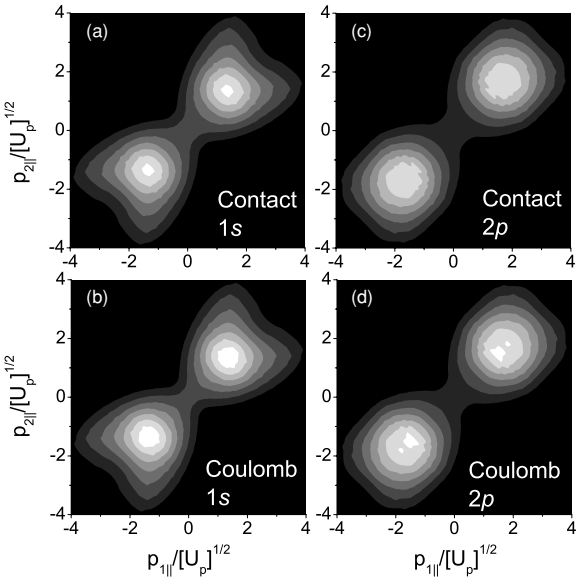

Figure 11. Electron-momentum distributions computed with the modified form factors (35) and (36), as functions of the electron-momentum components parallel to the laser-field polarization, for same field and atomic parameters as in the previous figures. We consider that the ionic potential is of contact type (equation (34)), and use the saddle-point model without modifications (cf section 2). In the upper and lower panels, the electron–electron interaction V_{12} was assumed to be of contact and Coulomb types, respectively. In panels (a) and (b), both electrons are taken to be initially in 1s states, whereas in panels (c) and (d), they are initially in 2p states. The transverse momenta have been integrated over.

Consequently, the yield in the diagonal gets enhanced. This is a feature shared with the limit for localized wavefunctions, so that the distributions are similar.

The subsequent figure (figure 11) is the counterpart of figure 10 for a contact-type ionic potential (equation (34)). In this case, for all types of electron–electron interaction V_{12} and initial bound states, the distributions are strongly localized near $p_{2||} = p_{1||} = \pm 2\sqrt{U_\mathrm{p}}$, even though their shapes are slightly different. This happens due to the fact that, in this case, $\eta(\mathbf{p}_j, \mathbf{k}) =$ constant. Therefore, the second terms in the form factors (35) and (36) are large near $p_{2||} = p_{1||} = \pm 2\sqrt{U_\mathrm{p}}$, but, in contrast to the Coulomb-potential case, no unequal momenta are favoured. This means that the inclusion of a short-range ionic potential leads to a radical improvement in the agreement between theory and experiment. In this context, for both the contact- and Coulomb-type interactions V_{12}, circular shapes reminiscent of those in the experiments are only obtained if we consider 2p states. As previously discussed, such states provide a more realistic description of the outer-shell electrons in neon, as compared to 1s states.

6. Conclusions

In this paper, we have introduced several technical modifications in an S-matrix theory of laser-induced nonsequential double ionization (NSDI), within the strong-field approximation, in which this phenomenon is modelled as the inelastic collision of an electron with its parent ion. Such modifications include different initial bound states for the first and second electrons, an adequate treatment of the bound-state singularity which exists in our framework and an

effective form factor which incorporates the residual ion. We performed a systematic analysis of their influence on the differential electron-momentum distributions as functions of the parallel-momentum components $p_{j||}$ ($j = 1, 2$) of both electrons.

Specifically, we consider that the second electron is dislodged by contact- and Coulomb-type interactions, and assume that both electrons are initially in a 1s, 2p or 3p hydrogenic state. As an additional case, we assume that the first electron is initially bound in a 1s state, and that the initial wavefunction of the second electron is localized at $\mathbf{r}_2 = 0$. For the first electron, we take into account only the hydrogenic states, since a neutral atom, in contrast to a singly ionized atom, has a long-range binding potential.

Concerning the initial bound-state wavefunction of the second electron, our results show that the NSDI momentum distributions are very sensitive to its spatial extension, but not to its shape. Indeed, a spatially extended wavefunction causes a broadening in the electron-momentum distributions along the anti-diagonal $p_{1||} = -p_{2||}$, even if the second electron is dislodged by a contact-type interaction. Circular-shaped distributions, as reported in [12, 13] and observed in experiments [1, 3], are only obtained for a contact-type interaction under the additional condition that the bound-state wavefunction is localized at the origin of the coordinate system, i.e., at $\mathbf{r}_2 = 0$. In addition to this broadening, if the second electron is released by a Coulomb-type interaction, there is an enhancement in the contributions near the axis $p_{1||} = 0$ or $p_{2||} = 0$.

All the distributions investigated in this paper, however, change in a less radical fashion if the second electron is taken to be in a 1s, 2p or 3p hydrogenic state, as long as they exhibit a spatial extension. In fact, although specific changes are observed, such as an additional substructure for a Coulomb-type interaction or more localized distributions for a contact-type interaction, the overall shapes of such distributions remain similar.

Furthermore, if the form factor $V_{\mathbf{k},0}$, which, within our model, contains all the influence of the initial state of the first electron, is incorporated in the time-dependent action, the only noticeable effect is a suppression in the yield, for regions of small parallel momenta. Indeed, the distributions retain their shapes even if the saddle-point equations are modified in this way. Such changes have been introduced in order to correct a singularity which exists for such a prefactor $V_{\mathbf{k},0}$, within the saddle-point framework, if the initial bound state is exponentially decaying.

Finally, the inclusion of the ionic potential at the time of rescattering, as the modified form factors $\widetilde{V}_{\mathbf{p}_j,\mathbf{k}}$, sheds some light on why, in the absence of the ion, a contact-type interaction localized at the origin of the coordinate system yields the best agreement with the experimental findings.

In fact, the ionic interaction leads to form factors which are very large near $p_{1||} = p_{2||} = \pm\sqrt{U_\mathrm{p}}$. This causes an enhancement in the distributions in this region. If the ionic potential is of Coulomb type, this effect is overshadowed by the fact that $\eta(\mathbf{p}_j, \mathbf{k})$, given by equation (22), favours unequal momenta. By contrast, if the ionic potential is given by equation (34), which is a good approximation for a short-range interaction, $\eta(\mathbf{p}_j, \mathbf{k}) =$ constant and the enhancement at the diagonal prevails. On the other hand, in sections 3 and 4, if $V_{\mathbf{p}_j,\mathbf{k}} =$ constant (i.e., for V_{12} of contact type and a localized state for the second electron), the very same effect is caused by integrating over the phase space. Interestingly, if, in the presence of the ion, we consider 2p states, which are more realistic assumptions for our model, the agreement with the experimental findings improves even more.

In conclusion, the present results indicate that the ionic potential is an important ingredient for a realistic modelling of NSDI. Indeed, of all the technical modifications considered in this paper, which aimed at making the model more realistic, this was the only which played a major role in improving the agreement between theory and experiment. The other modifications

either worsened this agreement or had almost no influence on the momentum distributions. This supports the hypotheses raised in previous studies [12, 13], that the residual ion might be screening both the long range of the Coulomb interaction or the final-state Coulomb repulsion, so that, effectively, the electron–electron interaction is of contact type, and the bound-state wavefunctions are localized.

We would like to stress out, however, that the treatment performed in section 5 is only a first approximation for a rigorous study of the ionic potential. There exist, in principle, more rigorous methods for incorporating the residual ion. The first approach would be to consider the ion as a further interaction in our model and modify the transition amplitude accordingly. This is, however, a highly non-trivial task, since it would lead to one more rescattering and a further integral in the transition amplitude. Another possibility would be to incorporate the ionic potential in the propagation of both electrons in the continuum. This would allow a clear assessment of the Coulomb focusing, which, again, owes its existence to the presence of the ion. Indeed, this effect may as well be compensating the broadening caused by initial spatially extended wavefunctions. Definite statements on this issue, however, require a theoretical approach beyond the strong-field approximation.

Acknowledgments

This work was financed in part by the Deutsche Forschungsgemeinschaft (SFB 407 and European Graduate College 'Interference and Quantum Applications'). We are grateful to A Sanpera for her collaboration in the initial stages of this project and to one of the referees for pointing out the possible role of the ionic potential. CFMF would like to thank the Optics Section at the Imperial College and City University for their kind hospitality and W Becker for useful discussions.

References

[1] See, e.g., Dörner R, Weber T, Weckenbrock W, Staudte A, Hattass M, Schmidt-Böcking H, Moshammer R and Ullrich J 2002 *Adv. At. Mol. Opt. Phys.* **48** 1
Ullrich J, Moshammer R, Dorn A, Dörner R, Schmidt L Ph H and Schmidt-Böcking H 2003 *Rep. Prog. Phys.* **66** 1463 for reviews on the subject
[2] Moshammer R *et al* 2000 *Phys. Rev. Lett.* **84** 447
Weber Th *et al* 2000 *Phys. Rev. Lett.* **84** 443
[3] Feuerstein B *et al* 2001 *Phys. Rev. Lett.* **87** 043003
Weber Th, Giessen H, Weckenbrock M, Urbasch G, Staudte A, Spielberger L, Jagutzki O, Mergel V, Vollmer M and Dörner R 2000 *Nature* **405** 658
[4] Corkum P B 1993 *Phys. Rev. Lett.* **71** 1994
Kulander K C, Schafer K J and Krause J L 1993 *Proc. of the SILAP Conference* ed B Piraux *et al* (New York: Plenum)
[5] Feuerstein B, Moshammer R and Ullrich J 2000 *J. Phys. B: At. Mol. Opt. Phys.* **33** L823
Chen J, Liu J, Fu L-B and Zheng W M 2000 *Phys. Rev.* A **63** 011404(R)
L-B Fu, Liu J, Chen J and Chen S-G 2001 *Phys. Rev.* A 043416
Chen J, Liu J and Chen S-G 2002 *Phys. Rev.* A **65** 021406(R)
Chen J, Liu J and Zheng W M 2002 *Phys. Rev.* A **66** 043410
[6] Haan S L, Wheeler P S, Panfili R and Eberly J H 2002 *Phys. Rev.* A **66** 061402(R)
Panfili R, Haan S L and Eberly J H 2002 *Phys. Rev. Lett.* **89** 113001
[7] Liu X and Figueira de Morisson Faria C 2004 *Phys. Rev. Lett.* **92** 133006
[8] Becker A and Faisal F H M 1994 *Phys. Rev.* A **50** 3256
[9] Becker A and Faisal F H M 2002 *Phys. Rev. Lett.* **89** 193003
Jaron A and Becker A 2003 *Phys. Rev.* A **67** 035401
[10] Kopold R, Becker W, Rottke H and Sandner W 2000 *Phys. Rev. Lett.* **85** 3781
Goreslavskii S P, Popruzhenko S V, Kopold R and Becker W 2002 *Phys. Rev.* A **64** 053402

Popruzhenko S V, Korneev Ph A, Goreslavskii S P and Becker W 2002 *Phys. Rev. Lett.* **89** 023001
Heinrich A, Lewenstein M and Sanpera A 2004 *J. Phys. B: At. Mol. Opt. Phys.* **37** 2087
[11] Figueira de Morisson Faria C and Becker W 2003 *Laser Phys.* **13** 1196
[12] Figueira de Morisson Faria C, Liu X, Becker W and Schomerus H 2004 *Phys. Rev.* A **69** 021402(R)
[13] Figueira de Morisson Faria C, Schomerus H, Liu X and Becker W 2004 *Phys. Rev.* A **69** 043405
[14] Figueira de Morisson Faria C, Liu X, Sanpera A and Lewenstein M 2004 *Phys. Rev.* A **70** 043406
[15] Keldysh L V 1964 *Zh. Éksp. Teor. Fiz.* **47** 1945
Keldysh L V 1965 *Sov. Phys. JETP* **20** 1307
Faisal F H M 1973 *J. Phys. B: At. Mol. Phys.* **6** L312
Reiss H R 1980 *Phys. Rev.* A **22** 1786
[16] Watson J B, Sanpera A, Lappas D G, Knight P L and Burnett K 1997 *Phys. Rev. Lett.* **78** 1884
Dundas D, Taylor K T, Parker J S and Smyth E S 1999 *J. Phys. B: At. Mol. Opt. Phys.* **32** L231
Liu W C, Eberly J H, Haan S L and Grobe R 1999 *Phys. Rev. Lett.* **83** 520
Szymanowski C, Panfili R, Liu W C, Haan S L and Eberly J H 2000 *Phys. Rev.* A **61** 055401
Lein M, Gross E K U and Engel V 2000 *Phys. Rev. Lett.* **85** 4707
[17] See, e.g., Salières P *et al* 2001 *Science* **292** 902
Becker W, Grasbon F, Kopold R, Milošević D B, Paulus G G and Walther H 2002 *Adv. At. Mol. Opt. Phys.* **48** 35 and references therein
[18] Yudin G L and Ivanov M Yu 2001 *Phys. Rev.* A **63** 033404
[19] Figueira de Morisson Faria C, Schomerus H and Becker W 2002 *Phys. Rev.* A **66** 043413
[20] Milošević D B and Becker W 2004 *Phys. Rev.* A **66** 063417
Sansone G, Vozzi C, Stagira S and Nisoli M 2004 *Phys. Rev.* A **70** 013411
Chipperfield L E, Gaier L N, Knight P L, Marangos J P and Tisch J W G 2005 *J. Mod. Opt.* **52** 243
[21] Bleistein N and Handelsman R A 1986 *Asymptotic Expansions of Integrals* (New York: Dover)
Schomerus H and Sieber M 1997 *J. Phys. A: Math. Gen.* **30** 4537
[22] This effect can be described employing the Hartree–Fock approximation to compute bound states of neon or argon. For a discussion of this method, see, e.g., Bethe H and Salpeter E E 1997 *Quantum Mechanics of One and Two Electron Atoms* (New York: Plenum)
For applications of HF potentials for time-dependent problems, see Kulander K C 1987 *Phys. Rev.* A **36** 2726
Kulander K C 1988 *Phys. Rev.* A **38** 777
Pindzola M S, Griffin D C and Bottcher C 1991 *Phys. Rev. Lett.* **66** 2305